J. Fluid Mech. (1975), *vol.* 69, *part* 4, *pp.* 705–719
Printed in Great Britain

Viscous incompressible flow between concentric rotating spheres. Part 3. Linear stability and experiments

By B. R. MUNSON

Department of Engineering Science and Mechanics, Engineering Research Institute, Iowa State University, Ames

AND M. MENGUTURK

Department of Mechanical Engineering, Duke University, Durham, North Carolina

(Received 26 June 1974)

The stability of flow of a viscous incompressible fluid contained between a stationary outer sphere and rotating inner sphere is studied theoretically and experimentally. Previous theoretical results concerning the basic laminar flow (part 1) are compared with experimental results. Small and large Reynolds number results are compared with Stokes-flow and boundary-layer solutions. The effect of the radius ratio of the two spheres is demonstrated. A linearized theory of stability for the laminar flow is formulated in terms of toroidal and poloidal potentials; the differential equations governing these potentials are integrated numerically. It is found that the flow is subcritically unstable and that the observed instability occurs at a Reynolds number close to the critical value of the energy stability theory. Observations of other flow transitions, at higher values of the Reynolds number, are also described. The character of the stability of the spherical annulus flow is found to be strongly dependent on the radius ratio.

1. Introduction

We consider here the flow of a viscous incompressible fluid contained between concentric spherical surfaces. The inner sphere rotates at a constant angular velocity within the stationary outer spherical surface. In particular, we consider the instability of the basic laminar flow from the standpoint of linear stability theory and present various experimental results regarding this flow. The basic laminar flow for the spherical annulus geometry shown in figure 1 is discussed in part 1 (Munson & Joseph 1971 *a*) and the stability of this motion from the standpoint of the energy stability theory is discussed in part 2 (Munson & Joseph 1971 *b*).

The linear stability problem for the basic flow of part 1 is considered here and a critical Reynolds number Re_L is determined. When $Re > Re_L$, the basic flow is unstable. The Reynolds number is defined as $Re = \Omega_1 R_2^2/\nu$, where R_2 is the radius of the outer sphere, Ω_1 is the angular velocity of the inner sphere and ν is the kinematic viscosity of the fluid. The linear-theory results are compared with the energy-theory results of part 2. Experimental results are compared with the

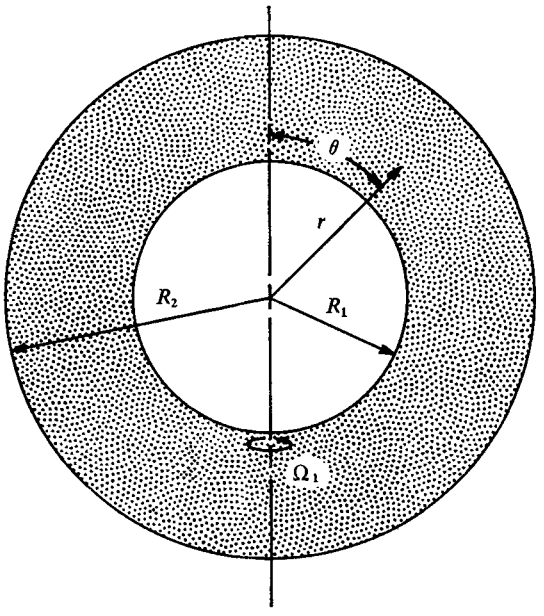

FIGURE 1. Spherical annulus geometry. $\eta = R_1/R_2$.

theoretical stability results as well as with various theoretical results concerning the basic laminar flow.

Others have carried out both theoretical and experimental investigations of flow in a spherical annulus. There are some results for narrow-gap geometry ($\eta \equiv R_1/R_2 \approx 1$), but results for wide-gap geometry ($\eta \ll 1$), which are more difficult to obtain, are sparse.

Yakushin (1969, 1970), Khlebutin (1968) and Zierep & Sawatzki (1970) have carried out approximate linear stability calculations for the narrow-gap case and have done experiments verifying the theory. In general, when the gap is narrow ($\eta \approx 1$) the first instability occurs as Taylor-type vortices in the region near the equator with other more complex transitions occurring at larger Reynolds numbers. Sawatzki & Zierep (1970) and Morales-Gomez (1974) present photographs of these instabilities as well as various other flow modes for sufficiently large Reynolds numbers.

On the other hand, Bratukhin (1961) obtained an approximate linear stability limit for wide-gap spherical annulus flow ($\eta = 0{\cdot}5$) by using the Stokes-flow approximation as the basic laminar flow. This approximation is valid only for sufficiently small Re (part 1). He found that $Re_L \approx 400$. We shall show that, if the proper basic flow is considered, a more accurate theoretical result with $\eta = 0{\cdot}5$ is $R_L \approx 1300$. Sorokin, Khlebutin & Shaidurov (1966) attempted to verify experimentally Bratukhin's result for $\eta = 0{\cdot}5$ but were unable to observe transitions indicating instability. A similar lack of any evidence of instability in the flow in a wide-gap spherical annulus was obtained by Khlebutin (1968) for $\eta < 0{\cdot}7$. The accurate experimental results for $\eta = 0{\cdot}44$ in the current study show that the first instability is subcritical. That is, the flow is unstable for $Re < Re_L$.

The basic laminar flow in a spherical annulus is a function of two spatial variables, r and θ, and in non-dimensional form is strongly dependent on the Reynolds number (see part 1). This Reynolds number dependence makes the study of flow between spheres different from, and possibly more typical of the general situation than, conventional problems like Poiseuille or Couette flow, which are independent of Reynolds number.

2. Formulation of linear stability theory

We consider the linear stability of the basic laminar flow in the spherical annulus. We superpose infinitesimal disturbances on the basic laminar flow and seek the conditions under which these small disturbances grow (unstable) or die out (stable). Thus, linear theory provides a critical Reynolds number Re_L such that if $Re > Re_L$ the flow is definitely unstable. On the other hand, energy theory provides a critical Reynolds number Re_E such that if $Re < Re_E$ the flow is definitely stable (to large or small disturbances). That is, energy theory gives sufficient conditions for stability and linear theory gives sufficient conditions for instability. Necessarily $Re_E \leqslant Re_L$, with the stability of the flow for $Re_E < Re < Re_L$ unknown. If the flow is unstable for Reynolds numbers in this range (sublinear or subcritical instability), it follows that the disturbances causing the instability must be of finite size.

The linear theory starts with the linearized Navier–Stokes equations, which may be written as

$$\left.\begin{aligned} \partial\mathbf{u}/\partial t + \mathbf{u}.\nabla\mathbf{U} + \mathbf{U}.\nabla\mathbf{u} &= -\nabla p + Re^{-1}\nabla^2\mathbf{u}, \\ \nabla.\mathbf{u} &= 0 \quad \text{in} \quad \mathscr{V}, \end{aligned}\right\} \tag{1}$$

with boundary conditions $$\mathbf{u} = 0 \quad \text{on} \quad \partial\mathscr{V}. \tag{2}$$

Here $\mathbf{u}$ is the arbitrary infinitesimal disturbance, $\mathscr{V}$ is the volume occupied by the fluid ($\eta \leqslant r \leqslant 1$, $0 \leqslant \theta \leqslant \pi$, $0 \leqslant \phi \leqslant 2\pi$) and $\partial\mathscr{V}$ the boundary of $\mathscr{V}$. The equations are in dimensionless form; R_2 is the characteristic length and Ω_1 is the characteristic angular velocity. The basic laminar flow $\mathbf{U} = (U_r, U_\theta, U_\phi)$, consisting of the primary flow (given by U_ϕ) and the secondary flow (given by U_r, U_θ), may be written as (see part 1)

$$U_r = (\partial\psi/\partial\theta)/r^2\sin\theta, \quad U_\theta = (-\partial\psi/\partial r)/r\sin\theta, \quad U_\phi = \Omega/r\sin\theta,$$

where $$\Omega(r,\theta) = \sum_s \sin^2\theta\, P_s(\theta) f_s(r), \quad \psi(r,\theta) = \sum_s \sin^2\theta\, P_s(\theta) g_s(r). \tag{3}$$

Here $P_s = P_s(\theta)$ is the Legendre polynomial of order s, a prime indicates d/dr and a dot indicates $d/d\theta$. The component functions $f_s(r)$ and $g_s(r)$ are obtained in part 1 by either a high-order perturbation solution or by a numerical integration. The number of functions needed to describe the basic flow accurately depends on the Reynolds number.

The problem, therefore, is to determine the critical value Re_L for (1) and (2) using the basic flow given by (3). The stability analysis is made difficult by the following facts. First, because the basic flow is a function of two spatial co-

ordinates (r and θ), the governing eigenvalue problem consists of partial differential equations. (For simpler problems the basic flow is a function of one co-ordinate and the governing equations can be reduced to ordinary differential equations.) Second, because of the nonlinear terms in the Navier–Stokes equations, the basic flow cannot be determined exactly but is known only as a series approximation as in (3). Thus the linear stability problem is solved using an appropriate series representation and numerical integration. A similar technique was used for the energy theory in part 2.

Although the physical interpretations and origins of the linear- and energy-theory stability problems are entirely different, the structures of the governing eigenvalue problem for each are superficially similar. Hence, the method used to solve for Re_E in part 2 is extended and used to solve for Re_L. This procedure is outlined briefly below.

The time dependence of the disturbances can be separated from their spatial dependence by using $\mathbf{u}(\mathbf{r}, t) = \mathbf{u}(\mathbf{r})\, e^{-\lambda t}$. The idea is to determine the lowest Reynolds number of the basic flow such that the real part of λ is zero (neutral disturbances). Any solenoidal vector $\mathbf{u}$ can be written in terms of its toroidal and poloidal components $\mathbf{T}$ and $\mathbf{S}$, respectively, as $\mathbf{u} = \mathbf{T} + \mathbf{S}$, where $\mathbf{T}$ and $\mathbf{S}$ are defined by their generating scalars Ψ and Φ as

$$\mathbf{T} = \operatorname{curl}(\Psi \mathbf{r}/r), \quad \mathbf{S} = \operatorname{curl}[\operatorname{curl}(\Phi \mathbf{r}/r)] \tag{4}$$

(see part 2; Chandrasekhar 1961, p. 622). These generating scalars can then be expanded in terms of spherical harmonics $Y_l^m(\theta, \phi)$, with the resulting representation for the arbitrary disturbances $\mathbf{u}$

$$\mathbf{u} = \sum_l \sum_m \left\{ \frac{l(l+1)}{r^2} S_l^m Y_l^m, \frac{1}{r} S_l^{m\prime} Y_l^m + \frac{im}{r \sin\theta} T_l^m Y_l^m, \frac{im}{r \sin\theta} S_l^{m\prime} Y_l^m - \frac{1}{r} T_l^m Y_l^m \right\}. \tag{5}$$

The component functions $T_l^m(r)$ and $S_l^m(r)$ of the disturbance flow must be such that the disturbance given by (5) satisfies the eigenvalue problem (1) with (2). It is necessary, of course, to truncate the series representation at some appropriate value $l = L_t$.

The systems of equations governing $T_l^m(r)$ and $S_l^m(r)$ are obtained as indicated below. Details are given by Menguturk (1974). We substitute the toroidal–poloidal representation (5) into the linearized Navier–Stokes equations (1), multiply by appropriate toroidal–poloidal functions whose scalar generators are unity and integrate over the unit sphere. After use of various orthogonality properties of toroidal–poloidal vectors and considerable algebra, the governing equations may be written in the following form:

$$\left.\begin{aligned} L_{l-1}^2 T_{l-1}^m - Re\, A_l^m \Sigma [G_4 S_{n-1}^{m\prime\prime} + G_1 S_{n-1}^{m\prime} + G_2 S_{n-1}^m + G_5 T_{n-1}^{m\prime} + G_3 T_{n-1}^m] = 0, \\ L_{l-1}^4 S_{l-1}^m - Re\, A_l^m \Sigma [H_6 S_{n-1}^{m\prime\prime\prime} + H_1 S_{n-1}^{m\prime\prime} + H_2 S_{n-1}^{m\prime} + H_3 S_{n-1}^m + H_7 T_{n-1}^{m\prime\prime} \\ + H_4 T_{n-1}^{m\prime} + H_5 T_{n-1}^m] = 0, \end{aligned}\right\} \tag{6}$$

where $L_{l-1}^2 = d^2/dr^2 - l(l-1)/r^2$. The structures of these equations and the energy equations of part 2 are similar. Here the various coefficients $G_j = G_{jnl}$ and

$H_j = H_{jnl}$ are functions of the component functions f_s and g_s of the basic flow:

$$G_1 = \frac{1}{r^2}\sum_s \alpha_1 f_{s-1}, \quad G_2 = \frac{1}{r^2}\sum_s (\alpha_2 f'_{s-1} + i\alpha_3 g''_{s-1}), \tag{7a,b}$$

$$G_3 = \frac{1}{r^2}\left[\sum_s (i\alpha_4 f_{s-1} + \alpha_5 g'_{s-1}) - \alpha_6 \lambda r^2\right], \quad G_4 = \frac{1}{r^2}\sum_s i\alpha_7 g_{s-1}, \quad G_5 = \frac{1}{r^2}\sum_s \alpha_8 g_{s-1}, \tag{7c–e}$$

$$H_1 = \frac{1}{r^2}\left[\sum_s \left(i\beta_1 f_{s-1} + \beta_2 g'_{s-1} + \frac{\beta_3 g_{s-1}}{r}\right) - \beta_4 \lambda r^2\right], \tag{7f}$$

$$H_2 = \frac{1}{r^2}\sum_s \left(i\beta_5 f'_{s-1} + \frac{i\beta_6 f_{s-1}}{r} + \beta_7 g''_{s-1} + \frac{\beta_8 g'_{s-1}}{r} + \frac{\beta_9 g_{s-1}}{r^2}\right), \tag{7g}$$

$$H_3 = \frac{1}{r^2}\left[\sum_s \left(i\beta_{10} f''_{s-1} + \frac{i\beta_{11} f'_{s-1}}{r} + \frac{i\beta_{12} f_{s-1}}{r^2} + \beta_{13} g'''_{s-1} + \frac{\beta_{14} g''_{s-1}}{r} + \frac{\beta_{15} g'_{s-1}}{r^2} + \frac{\beta_{16} g_{s-1}}{r^3}\right) - \beta_{17}\lambda\right], \tag{7h}$$

$$H_5 = \frac{1}{r^2}\sum_s \left(\beta_{22} f'_{s-1} + \frac{\beta_{23} f_{s-1}}{r} + i\beta_{24} g''_{s-1} + \frac{i\beta_{25} g'_{s-1}}{r} + \frac{i\beta_{26} g_{s-1}}{r^2}\right), \tag{7i}$$

$$H_6 = \frac{1}{r^2}\sum_s \beta_{27} g_{s-1}, \quad H_7 = \frac{1}{r^2}\sum_s i\beta_{28} g_{s-1}. \tag{7j,k}$$

The numerous coefficients $\alpha_j \equiv \alpha_{jlsm}$ and $\beta_j \equiv \beta_{jlsm}$ are evaluated by Munson (1970) and Menguturk (1974) in terms of integrals of triple products of various spherical harmonics and their derivatives. The integers N_t and L_t indicate the order of truncation for the basic flow series (3) and the disturbance flow series (5).

The wavenumber m determines the symmetry of the disturbances about the axis of rotation and affects the character of the governing equations. For example, with $m = 0$ (axisymmetric disturbances) and real values of λ (exchange of stability) the eigenvalue problem (1) with (2) is completely real. On the other hand, for $m \neq 0$ (non-axisymmetric disturbances) or λ complex (oscillatory disturbances) the equations are complex and must be written in terms of real and imaginary parts. Only real values of λ are considered in this study.

The task is to determine the smallest value of Re for which $\lambda = 0$. The procedure is as follows. Given η, select Re; this specifies the parameter Re in the governing equations as well as the component functions f_s and g_s of the basic flow, which are implicit functions of Re and η. If axisymmetric disturbances are of interest, $m = 0$, and the governing system is integrated numerically to obtain the minimum eigenvalue Re_L. The first zero of the curve $\lambda = \lambda(Re)$ defines the critical value Re_L; $\lambda(Re_L) = 0$. Non-axisymmetric disturbances, $m \neq 0$, are treated in the same manner.

It is noted that the general disturbances represented by (5) and determined by the governing equations (6) can be considered as the sum of two separate types: disturbances symmetric or antisymmetric with respect to the equator. Mathematically this consists of using toroidal–poloidal components T_i and S_j with i odd and j even or i even and j odd. (A similar technique was used by

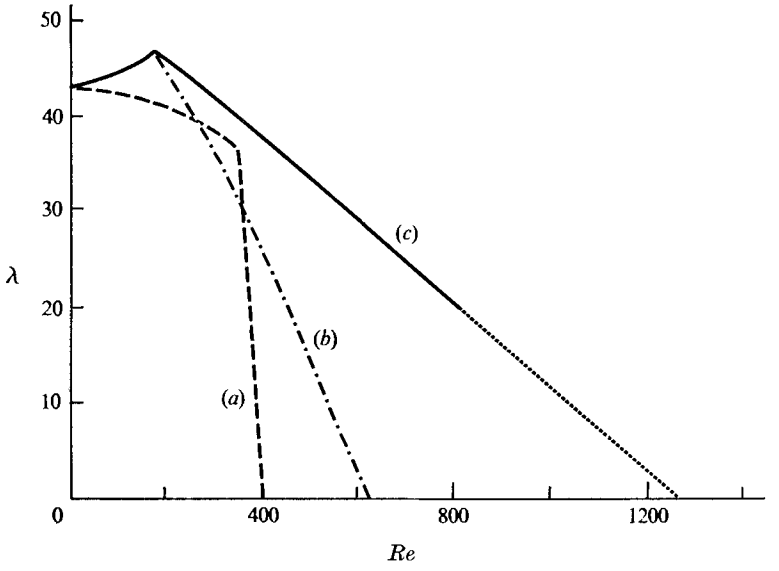

FIGURE 2. Linear-theory eigenvalue as a function of Reynolds number for $\eta = 0{\cdot}5$: $\mathbf{u} = \mathbf{u}(\mathbf{r})e^{-\lambda t}$. – –, Bratukhin's (1961) approximate result; — – —, this study with Stokes flow as basic flow; ——, this study with accurate basic flow.

Bratukhin (1961) for his approximate solution.) The minimum eigenvalue of the general problem is the minimum eigenvalue of these two separate problems.

3. Linear-theory stability results

Results of the linear stability analysis outlined above are discussed below for $\eta = 0{\cdot}5$. We compare the results of this research with other approximate results. As mentioned previously, Bratukhin (1961) obtained an approximate result for axisymmetric disturbances ($m = 0$) by using the Stokes-flow approximation as the basic flow and a perturbation technique (up to second-order terms in Re) for the stability problem. (It is noted that the difference between the actual basic flow and the Stokes-flow approximation becomes larger as Re increases; see §4.) The result of Bratukhin's approximate stability analysis, shown in figure 2 as curve (*a*), indicates that $Re_L \approx 400$. This curve consists of two distinct segments given by $\lambda = \min[150(1-\frac{1}{404}Re)^2, 43{\cdot}2(1-\frac{1}{904}Re)^2]$, corresponding to different modes of disturbance.

A better, but not final, approximation to the critical Reynolds number Re_L is obtained by solving the eigenvalue problem developed above with Stokes flow as the basic flow. This $\lambda = \lambda(Re)$ curve, shown in figure 2 as curve (*b*), yields a value of Re_L of 630. It is noted that a seventh-order disturbance flow truncation, $L_t = 7$, provided sufficient convergence of the series shown in (5).

Curve (*c*) of figure 2 gives the stability characteristics when the correct basic flow is considered. The basic flow is represented by functions f_l and g_l with $l \leqslant 7$ and the disturbance flow is truncated at $N_t = 7$. It is seen that the value of Re_L is increased from the values 400 and 630 for Stokes-flow approximations to

$Re_L \approx 1300$ for the accurate representation of the basic flow. This curve (as well as curves (*a*) and (*b*)) consists of two distinct segments corresponding to different modes of disturbance. That is, the minimum eigenvalue does not correspond to the same disturbance mode for all Reynolds numbers. The dotted portion of the curve is an extrapolation to the value $\lambda = 0$. This extrapolation is necessary since it was not possible to obtain the basic flow accurately for $Re > 900$. That is, as indicated in part 1, for large Re numerical difficulties were encountered in the integration of the system of nonlinear ordinary differential equations governing the basic flow.

It is of interest to note that the disturbance flow corresponding to the critical Reynolds number ($\lambda(Re_L) = 0$) is not symmetric with respect to the equator. However, it is axisymmetric ($m = 0$). Thus, according to this linear theory, the disturbance flow is different from the basic flow in that there is a distinct flow between the northern and southern hemispheres. The disturbance flow according to energy theory is also asymmetric with respect to the equator (part 2). In addition, it is non-axisymmetric ($m \neq 0$). Contrary to this, experimental results discussed below show no evidence of antisymmetric flow.

The basic flow is a function of the Reynolds number. Hence the curves $\lambda = \lambda(Re)$ for the Stokes basic flow are different from that for the accurate basic flow. For small Re, curves (*b*) and (*c*) nearly coincide. However, as Re becomes larger the difference becomes significant. It is of interest to know what characteristics of the basic flow are responsible for this increased stability.

To study the effects of separate parts of the basic flow, the stability of various pseudo basic flows was considered. For example, a pseudo basic flow consisting of the accurate primary motion (flow about the axis of rotation) and the approximate Stokes secondary motion (flow in the meridian plane) was considered. Other combinations were also considered. The results can be summarized as follows. When the Reynolds number is increased, the streamlines of the secondary basic flow change their shape (see part 1). The centre of the secondary swirl moves closer to the equator (producing a greater jetting of the fluid from the equator of the inner sphere). This change causes the flow to become more unstable. On the other hand, the fact that as the Reynolds number is increased the angular-velocity contours of the primary flow deviate from spheres (which characterize level surfaces at low Reynolds number) causes the flow to become more stable. The net result of the changes in the character of the basic flow as the Reynolds number is increased is an increase in the stability of the flow (as shown by curves (*b*) and (*c*) in figure 2).

A summary of the stability results for flow between a rotating inner sphere and a stationary concentric outer sphere is shown in figure 3. Both the linear and energy stability limits are shown as a function of radius ratio. The theoretical results for the small-gap situation ($\eta \approx 1$) are those of Yakushin (1969), who used Stokes flow as the basic flow and a Galerkin-type solution of the stability problem. The large-gap results ($\eta = 0{\cdot}5$) are from the present study as well as Bratukhin's perturbation solution. Energy-theory results for $\eta = 0{\cdot}5$ and $0{\cdot}75$ are also shown (part 2). The various experimental results shown in figure 3 are discussed in the next section.

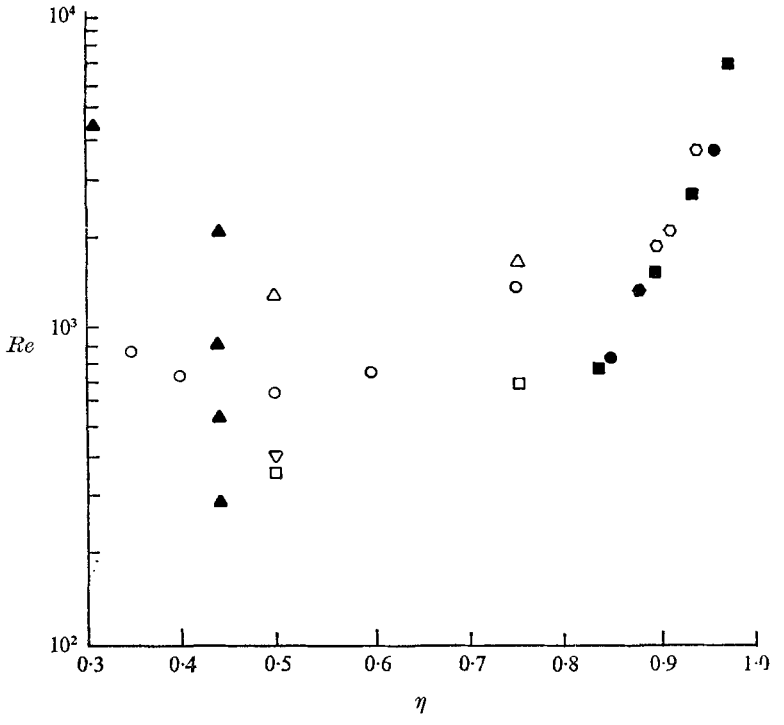

FIGURE 3. Theoretical and experimental stability results for spherical annulus flow with stationary outer sphere. Linear theory: △, this study, accurate basic flow; ○, this study, Stokes flow; ▽, Bratukhin (1961); ⬭, Yakushin (1969). Energy theory: □, Munson & Joseph (1971*b*). Experiment: ▲, ⬮, this study; ■, Khlebutin (1968); ●, Sawatzki & Zierep (1970).

It is noted that for $\eta \approx 1$ the flow near the equator can be thought of as being similar to the flow between rotating cylinders. Thus, as mentioned by Khlebutin (1968), the stability results for narrow-gap spherical annulus flow are quite similar to those for narrow-gap Taylor flow (rotating cylinders). However, as the gap width increases, the correspondence between the spherical annulus and the cylindrical annulus vanishes.

4. Experimental results

The apparatus shown schematically in figure 4 was used to obtain experimental results regarding various aspects of the flow in a spherical annulus. These included torque measurements and results of flow-visualization experiments for a wide range of Reynolds numbers with radius ratios of $\eta = 0{\cdot}881$ (narrow gap), 0·440 (wide gap) and 0·304 (very wide gap).

The main components of the experimental apparatus are (*b*) a clear outer spherical shell of diameter $12{\cdot}95 \pm 0{\cdot}05$ cm, (*a*) an inner sphere rotated by a variable-speed electric motor, (*d*) a torsion wire from which the Plexiglas box containing the outer sphere is suspended, a means of measuring the angular rotation of the outer sphere (in order to determine the applied torque) and

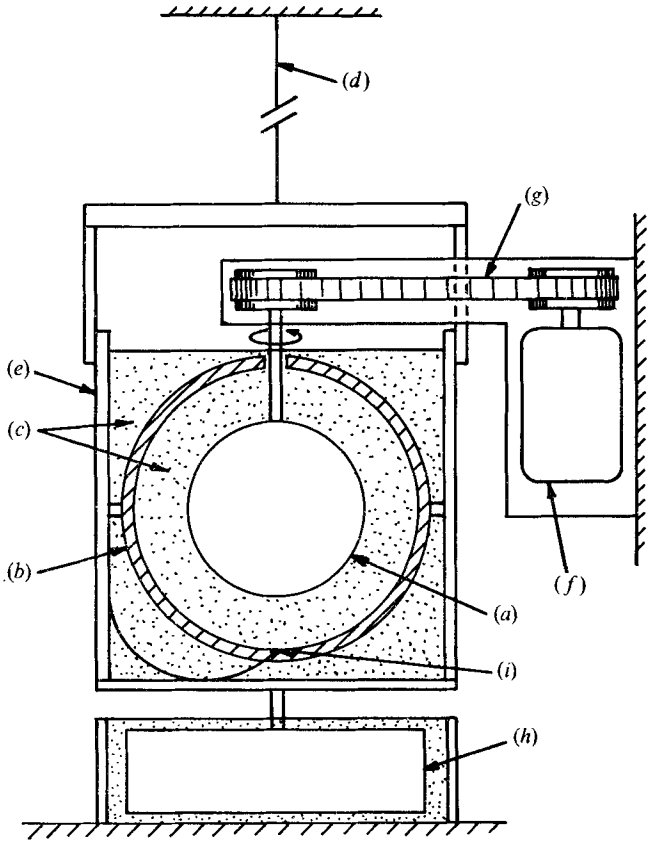

FIGURE 4. Schematic diagram of experimental apparatus for spherical annulus flow. (*a*) Rotating inner sphere. (*b*) Stationary outer sphere. (*c*) Silicone oil. (*d*) Torsion wire connected to outer sphere. (*e*) Plexiglas box. (*f*) Variable-speed motor. (*g*) Belt drive. (*h*) Viscous damper. (*i*) Thermocouple.

(*i*) a thermocouple to measure the temperature of the fluid in the annulus. Silicone oils of various viscosities (10–1000 cS) were used as the fluid. Speed regulation of the inner sphere was excellent. Small random fluctuations in angular velocity ($\pm 0{\cdot}25\,\%$) produced noticeable changes in the torque. Data were not taken during such oscillations. In order to reduce optical distortion, the region between the outside of the outer sphere and the Plexiglas box holding this sphere was filled with fluid also. Torques were determined by using a torsion wire of known spring constant. Flow visualization was carried out by using either aluminium flakes suspended in the fluid or dye injection.

4.1. *Basic flow*

Flow-visualization studies confirmed that the basic flow was as given by the theoretical results of part 1 and others (Pearson 1967). Figures 5 and 6 (plates 1 and 2) show typical streamlines for three radius ratios. The secondary flows are clearly visible. The streamlines were made visible by injecting a finite spot of

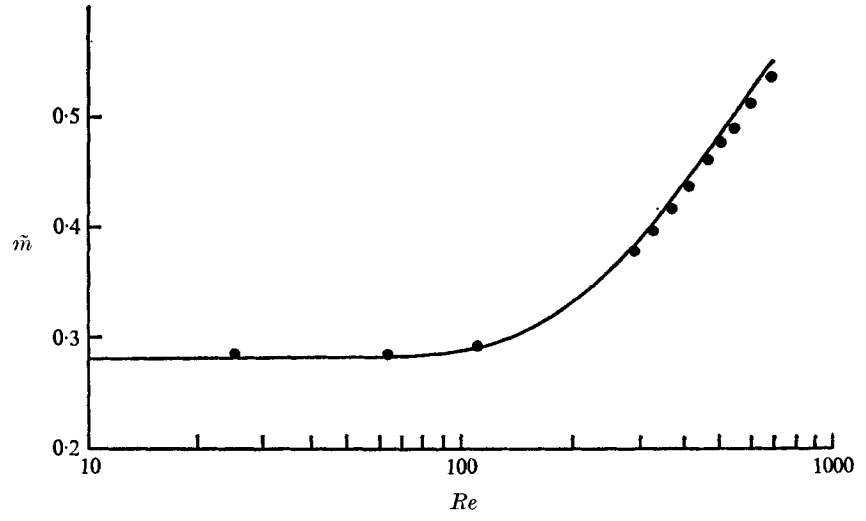

FIGURE 7. Torque as a function of Reynolds number for $\eta = 0{\cdot}440$ and outer sphere stationary. ●, experimental results; ——, theoretical torque for basic laminar flow, Munson & Joseph (1971*a*).

neutrally buoyant dye within the annulus and allowing it to be stretched out as the flow proceeded. It is seen that, at the low Reynolds numbers shown, the fluid makes many revolutions about the axis of rotation before completing one secondary flow circuit.

The theoretical torque M needed to rotate the inner sphere was obtained in part 1. The dimensionless torque

$$\tilde{m}(Re, \eta) = 3M/(8\pi\mu\Omega_1 R_2^3)$$

is a function of the Reynolds number. For small Re, when secondary flows are not important, $\tilde{m}$ is independent of Re. For larger Reynolds numbers, when the secondary flow becomes important, the torque becomes larger than the limiting Stokes-flow value. Figure 7 (for $\eta = 0{\cdot}44$) shows the good agreement between theory (Stokes-flow limit and larger Reynolds number basic flow solution of part 1) and experiment.

The limiting case $\eta \to 0$ corresponds to the flow induced by the rotation of a single sphere in an unbounded fluid. It is of interest to determine the effect of a stationary outer bounding sphere of finite radius by considering the effect of η. For this situation we redefine the Reynolds number so that

$$\widehat{Re} = R_1^2 \Omega_1/\nu = \eta^2 Re$$

and the dimensionless torque so that

$$\hat{m} = M/\mu R_1^3 \Omega_1 = (8\pi/3\pi^3)\,\tilde{m}.$$

The low Reynolds number solution (Stokes flow, see part 1) then gives $\hat{m} = 8\pi/(1-\eta^3)$ as $\widehat{Re} \to 0$. The large Reynolds number solution (boundary layer) for the case $\eta = 0$ has been determined by Howarth (1954) as $\hat{m} = 3{\cdot}32\,\widehat{Re}^{\frac{1}{2}}$. This relationship between the torque and Reynolds number has been confirmed experimentally to within 10 % by Bowden & Lord (1963).

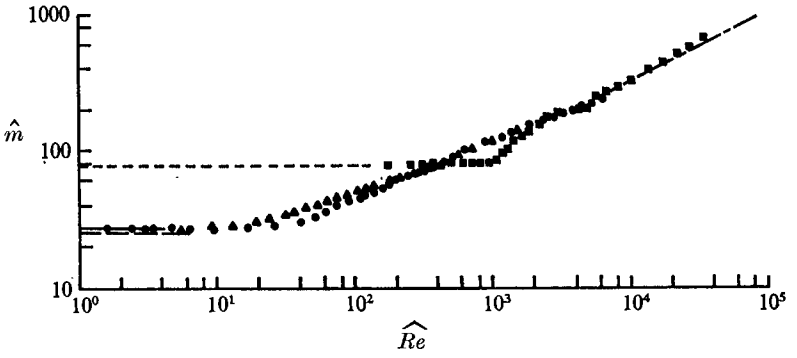

FIGURE 8. Torque as a function of Reynolds number for different radius ratios. Experimental results: ▲, $\eta = 0{\cdot}304$; ●, $\eta = 0{\cdot}440$; ■, $\eta = 0{\cdot}881$. Theory: – –, Stokes flow, $\eta = 0{\cdot}304$; ——, Stokes flow, $\eta = 0{\cdot}440$; ----, Stokes flow, $\eta = 0{\cdot}881$; —·—, boundary layer, $\eta = 0$, Howarth (1954).

Experimental torque data for three different radius ratios are presented in figure 8 along with the theoretical results given above. It may be seen that for small enough Reynolds numbers the torque is independent of $\widehat{Re}$ and is given very accurately by the Stokes-flow torque formula. For these low Reynolds numbers, the torque is a strong function of the radius ratio, provided that η is not near zero.

It may be seen from figure 8 that the Reynolds number at which the character of the flow begins to deviate from that of Stokes flow is strongly dependent upon the radius ratio. For example, the dimensionless torque is constant for $\widehat{Re} \lesssim 900$ if $\eta = 0{\cdot}881$, for $\widehat{Re} \lesssim 20$ if $\eta = 0{\cdot}440$ and for $\widehat{Re} \lesssim 7$ if $\eta = 0{\cdot}304$. As discussed below, the Reynolds number for transition of the basic laminar flow to another laminar flow or turbulence is also a strong function of η.

On the other hand, for large $\widehat{Re}$ the dimensionless torque is essentially independent of η, at least for the range of radius ratios considered in this study ($0{\cdot}304 \leqslant \eta \leqslant 0{\cdot}881$). Within this range of η the torque is given quite well by Howarth's $\eta = 0$ boundary-layer solution. Thus, for large $\widehat{Re}$ the relatively thin boundary layer apparently determines the torque required to rotate the sphere quite independently of the radius of the stationary outer sphere (even for the narrow-gap situation with $\eta = R_1/R_2 = 0{\cdot}881$).

For a given inner sphere, angular velocity and fluid, it may be expected that the torque would increase if the gap size were made smaller (the outer-sphere radius reduced). Such is the case for small $\widehat{Re}$ ($\hat{m}$ increases with η in the Stokes-flow limit). For large $\widehat{Re}$ the torque is essentially independent of η. However, for certain cases the torque may actually decrease as the gap size decreases. Such is the case for $\widehat{Re} = 10^3$ with $\eta = 0{\cdot}440$ or $0{\cdot}881$ (see figure 8). This characteristic results from the fact that the range of validity of the Stokes-flow condition increases rapidly with η and that the Reynolds number for transition (with the corresponding changes in torque characteristics) is also a function of η.

4.2. *Stability*

Sawatzki & Zierep (1970) and Khlebutin (1968) presented torque data indicating various flow transitions for narrow-gap geometry ($\eta \approx 1$). On the other hand, Sorokin *et al.* (1966) and Khlebutin (1968) were unable to detect any transitions (in either torque measurements or flow-visualization studies) for the wide-gap case ($\eta \lesssim 0{\cdot}7$). A summary of the various experimental stability results is shown in figure 3. We feel that the reason why break points (transitions) were not observed in wide-gap experiments prior to this one is that the character of the flow is strongly dependent on the radius ratio and the break is smaller when the gap is bigger. Hence very careful experiments were carried out.

The results of narrow-gap experiments of this study ($\eta = 0{\cdot}881$) are very similar to those previously reported in the literature. In particular, a series of transitions in the character of the flow was observed both visually, by using aluminium particles in the fluid, and from relatively large breaks in the torque curve $\tilde{m} = \tilde{m}(Re)$. The initial instability takes place in the form of Taylor vortices near the equator, with various other transitions occurring for Reynolds numbers above the critical value. A discussion and photographs of these various transitions for the narrow-gap case are given by Sawatzki & Zierep (1970) and Morales-Gomez (1974).

As mentioned above, other investigators were unsuccessful in observing any transitions in the flow for the wide-gap case. However, four break points (or transitions in the flow) were observed for the $\eta = 0{\cdot}440$ case of the current study. The second one, occurring at $Re = 540$, is shown in figure 9. Although the change in the torque curve is not large, a definite change in slope is apparent. Careful experiments showed that the data were repeatable within the narrow range indicated in the figure and free of hysteresis. The first and third break points, occurring at $Re = 290$ and $Re = 900$ for this radius ratio, produce similar torque characteristics. A fourth, and more pronounced, break occurred at $Re = 2100$. At this Reynolds number the flow suddenly becomes turbulent. The four transitions described above are indicated in figure 3.

According to energy stability theory (part 2), for $\eta = 0{\cdot}440$ and the outer sphere stationary, flow in a spherical annulus is stable to any disturbances (large or small) if $Re \lesssim Re_E = 310$. (This value is obtained by an extrapolation from the known results for $\eta = 0{\cdot}5$.) The close agreement between the critical value $Re = 310$ of energy theory and the first break point, $Re = 290$, is noteworthy. Since the linear theory indicates that $Re_L \approx 1300$, it appears that transition from the basic laminar flow is subcritical and, therefore, is caused by disturbances of finite size under circumstances in which infinitesimal disturbances decay.

Careful observations of the flow field by using aluminium flakes suspended in the fluid were made in order to observe the nature of the various transitions in the flow. As mentioned previously, other investigators observed various instabilities in the narrow-gap case, but did not observe any instabilities in the wide-gap case. In this investigation, for $\eta = 0{\cdot}440$ no instabilities were observed for Reynolds numbers encompassing the first break point in the torque curve. It is possible that the instabilities may occur in a form similar to the secondary motion

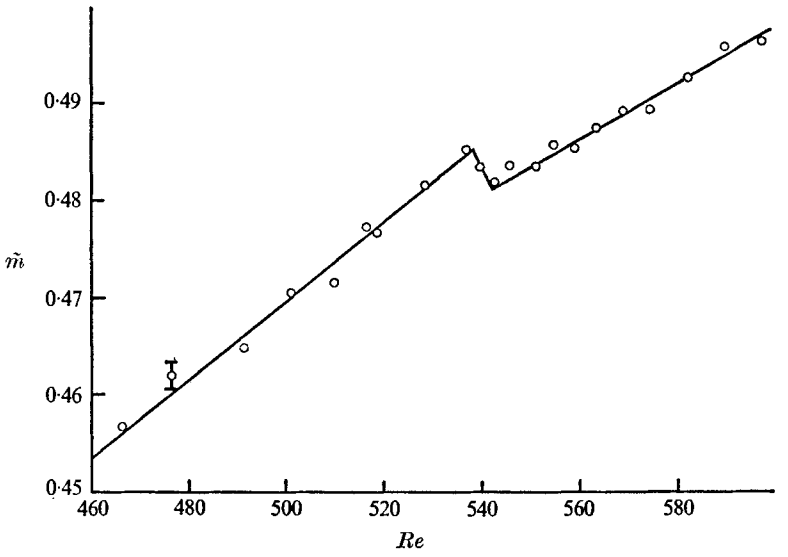

FIGURE 9. The second transition in the flow for $\eta = 0{\cdot}440$ indicated by the break in the torque as a function of Reynolds number. Data repeatable within the band shown.

of the basic flow and thus be indistinguishable from the basic flow, although they would produce the break in the torque curve. It is noted that the instabilities for Bratukhin's (1961) approximate linear analysis are of this form.

At the Reynolds number corresponding to the second break point ($Re = 540$ for $\eta = 0{\cdot}44$), an instability appears in the form of small spots or puffs of turbulence. These turbulent spots occur at the centre of the secondary basic flow swirl and rotate about the axis of rotation at a rate corresponding to the angular velocity of the primary flow at that location. At Reynolds numbers corresponding to the third break point, a slight waviness or unsteadiness is observed near the equator. This unsteadiness increases and spreads towards the poles as the Reynolds number is increased. Finally, for Reynolds numbers corresponding to the fourth break point ($Re = 2100$ for $\eta = 0{\cdot}44$), the flow suddenly becomes completely turbulent. It is noted that for the first three break points the break in the dimensionless torque curve occurs as a decrease in $\tilde{m}$, whereas the fourth break (transition to turbulence) occurs as an increase in $\tilde{m}$. It is also noted that the magnitudes of these breaks in the torque curve for this large-gap case are considerably smaller than those for the narrow-gap situation.

The experimental results for the annulus with a very wide gap ($\eta = 0{\cdot}304$) are different from those discussed above (for $\eta = 0{\cdot}881$ and $0{\cdot}44$) in that no transitions in the flow were observed until the flow became turbulent at $Re = 4600$. For Reynolds numbers below this value, neither torque measurements nor visualization studies indicated any flow transition. The transition to turbulence at $Re = 4600$ may easily be observed using flow-visualization techniques and torque measurements.

5. Summary and conclusions

Theoretical and experimental results regarding the flow in a spherical annulus bounded by a stationary outer sphere and a rotating inner sphere have been presented. Flow properties have been shown to be strongly dependent on the ratio of the radii of the two spherical surfaces and the Reynolds number.

The torque needed to rotate the inner sphere at a constant angular velocity is a function of the radius ratio and Reynolds number. For small Reynolds numbers the torque was found to agree very well with the theoretical Stokes-flow solution. In these cases the secondary flows are negligible, fluid inertia is small and the torque is proportional to the fluid viscosity and angular velocity (the dimensionless torque is independent of the Reynolds number).

For moderate Reynolds numbers the torque is a complex function of the radius ratio and Reynolds number. The effect of secondary flows (non-negligible inertia effects) is to increase the torque above that given by the Stokes-flow approximation (the dimensionless torque is an increasing function of the Reynolds number for moderate Reynolds numbers).

For large Reynolds numbers the flow assumes a boundary-layer character. For these cases the torque is essentially independent of the radius ratio and agrees very well with the results of boundary-layer theory for a rotating sphere in an unbounded fluid.

The stability of spherical annulus flow is strongly dependent on the radius ratio; not only quantitatively, but qualitatively as well. In particular, the transitions involved in the wide-gap situation do not involve the Taylor-type vortices of the narrow-gap case and are much less drastic and more difficult to detect. The instability is initiated as a sublinear one near the critical value of the energy theory. For the case of a very wide gap, transitions (except for the transition to turbulence), if present at all, were not detected.

The support of NSF Grant GK-35513 has been appreciated.

REFERENCES

BOWDEN, F. R. & LORD, R. G. 1963 The aerodynamic resistance of a sphere rotating at high speed. *Proc. Roy. Soc.* A **271**, 142.

BRATUKHIN, IU. K. 1961 On the evaluation of the critical Reynolds number for the flow between two rotating spherical surfaces. *J. Appl. Math. Mech.* **25**, 1286.

CHANDRASEKHAR, S. 1961 *Hydrodynamic and Hydromagnetic Stability*. Oxford University Press.

HOWARTH, L. 1954 Note on the boundary layer on a rotating sphere. *Phil. Mag.* **42**, 1308.

KHLEBUTIN, G. N. 1968 Stability of fluid motion between rotating and stationary concentric spheres. *Izv. Akad. Nauk SSSR, Mekh. Zh. i Gaza*, **3**, 1. (Trans. *Fluid Dyn.* **3** (1968), 6.)

MENGUTURK, M. 1974 Ph.D. thesis, Department of Mechanical Engineering, Duke University.

MORALES-GOMEZ, J. 1974 Ph.D. thesis, Department of Mechanical Engineering, New Mexico State University.

MUNSON, B. R. 1970 Ph.D. thesis, Department of Aerospace Engineering and Mechanics, University of Minnesota.

MUNSON, B. R. & JOSEPH, D. D. 1971*a* Viscous incompressible flow between concentric rotating spheres. Part 1. Basic flow. *J. Fluid Mech.* **49**, 289.

MUNSON, B. R. & JOSEPH, D. D. 1971*b* Viscous incompressible flow between concentric rotating spheres. Part 2. Hydrodynamic stability. *J. Fluid Mech.* **49**, 305.

PEARSON, C. E. 1967 A numerical study of the time-dependent viscous flow between two rotating spheres. *J. Fluid Mech.* **28**, 323.

SAWATZKI, O. & ZIEREP, J. 1970 Flow between a fixed outer sphere and a concentric rotating inner sphere. *Acta Mechanica*, **9**, 13.

SOROKIN, M. P., KHLEBUTIN, G. N. & SHAIDUROV, G. F. 1966 Study of the motion of a liquid between two rotating spherical surfaces. *J. Appl. Mech. Tech. Phys.* **6**, 73.

YAKUSHIN, V. I. 1969 The instability of the motion of a liquid in a thin spherical layer. *Izv. Akad. Nauk SSSR, Mekh. Zh. i Gaza*, **4**, 1. (Trans. *Fluid Dyn.* **4** (1972), 1.)

YAKUSHIN, V. I. 1970 Instability of the motion of a liquid between two rotating spherical surfaces. *Izv. Akad. Nauk SSSR, Mekh. Zh. i Gaza*, **5**, 4. (Trans. *Fluid Dyn.* **5** (1973), 4.)

ZIEREP, J. & SAWATZKI, O. 1970 Three dimensional instabilities and vortices between two rotating spheres. *8th Symp. on Naval Hydrodyn.*

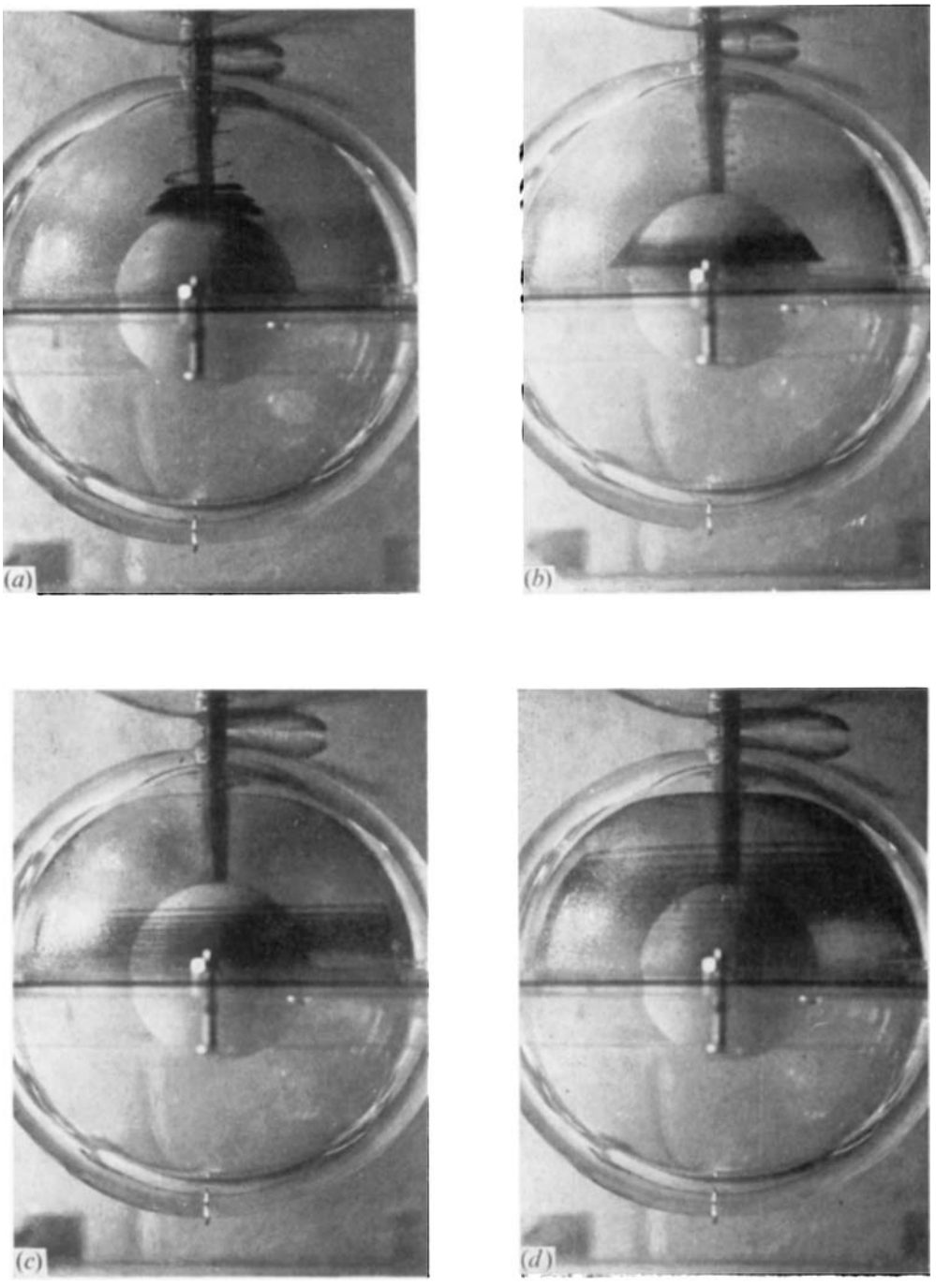

FIGURE 5. Basic flow as indicated by dye streaks for $\eta = 0{\cdot}44$ and $Re \approx 20$. Inner sphere rotating; outer sphere stationary. (*a*)–(*d*) are in time sequence.

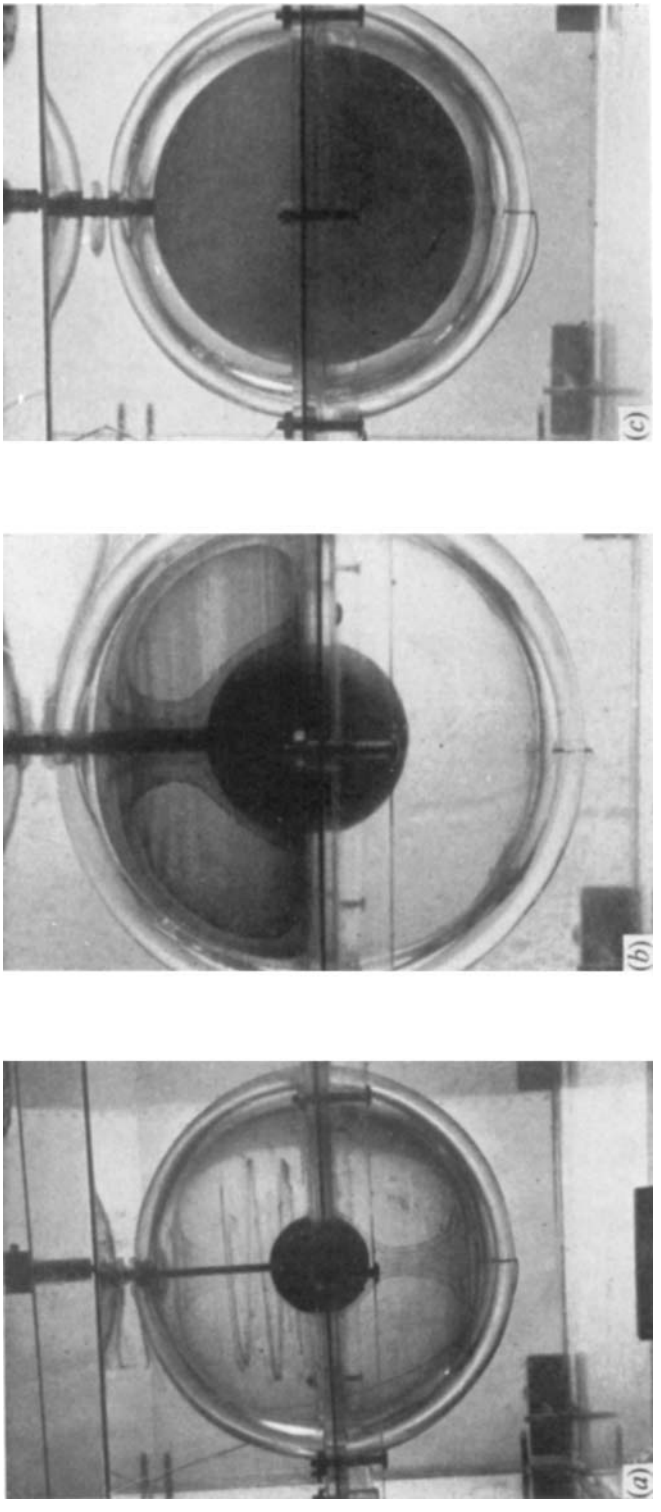

FIGURE 6. Basic flow as indicated by dye pattern for various radius ratios and $Re \approx 30$. Inner sphere rotating; outer sphere stationary. (*a*) $\eta = 0{\cdot}306$, (*b*) $\eta = 0{\cdot}440$, (*c*) $\eta = 0{\cdot}881$.